Fizika Nizkikh Temperatur, 2000, v. 26, Nos. 9/10, p. 909–917

Atomic oxygen in solid deuterium

A. V. Danilychev and V. A. Apkarian

Department of Chemistry, University of California, Irvine, California 92697-2025
E-mail: aapkaria@uci.edu

H. Kajihara, S. Tanaka, and S. Koda

Department of Chemical System Engineering, Faculty of Engineering, the University of Tokyo, Hongo 7-3-1, Bunkyo-ku, Tokyo 113, Japan

Received June 8, 2000

Atomic oxygen is photogenerated in solid D_2 by 193 nm irradiation of samples initially doped with molecular oxygen. The atoms are detected by laser induced fluorescence over the O ($^1S \rightarrow {}^1D$) transition, which occurs at 559 nm, with a fluorescence lifetime of 230 μs. The absorption leading to this emission is indirect, attributed to O_2 (X) : O (^3P) pairs. Complementary studies are carried in solid D_2 co-doped with Xe and O_2 , in which in addition to ionic XeO centers, the atomic O ($^1S \rightarrow {}^1D$) transition with a radiative lifetime of 50 μs is observed. The photogeneration of the atomic centers, and stability of atomic and molecular emissions, are sensitive to sample preparation and thermal and irradiation histories. In annealed solids, at temperatures below 6.5 K, the atomic emission does not bleach, implying that the vertically prepared O (^1D) atoms undergo intersystem crossing to form O (^3P) rather than react with D_2 . The barrier to insertion on the O (^1D) + D_2 potential energy surface in solid D_2 is explained as a many-body polarization effect. The recombination of O (^3P) atoms can be initiated thermally, and monitored by their thermoluminescence over the molecular O_2 ($A' \rightarrow X$) transition. The thermal onset of recombination varies between 5.5 K and 9 K, depending on the sample preparation method. In all cases, the thermally induced recombination is catastrophic, accompanied by thermal runaway, pressure burst, and material loss. This is interpreted as indication that the process is initiated by self-diffusion of the host, consistent with the notion that atomic O centers stabilize the host lattice.

PACS: 33.80.Gj, **78.55.–m**, 78.60.Kn

1. Introduction

Oxygen doped solid hydrogen, and its isotopes, provide an opportunity for the study of photophysics and chemistry in quantum hosts. In addition to fundamental motivations, solid hydrogen doped with atomic oxygen is a prototype of a mono-propellant, which with optimized dopant concentration, could have significantly enhanced specific impulse over the standard liquid oxygen/hydrogen mix presently used as rocket fuel [1]. The present study was motivated by the absence of the rudimentary data required to assess the possibility of this concept [2]. Our experimental studies show the stability of atomic oxygen with respect to diffusion, and more significantly, we uncover the non-reactivity of both ground and electronically excited atomic oxygen with the D_2 host. Reports of these findings have appeared as conference proceedings [3] and in a thesis [4]. Here, we collect some of the more important observations, which have served as the basis for theoretical analyses that have already been published [5,6].

The experimental plan is based on our prior studies of atomic and molecular oxygen in rare gas solids [7–9]. The in-situ photogeneration of atomic oxygen, by ArF laser irradiation of O_2-doped solid hydrogen at 193 nm, is the proposed starting point. Note, although this radiation provides energy 1.3 eV in excess of the dissociation limit of the molecule, in rare gas solids, a strong cage effect prevents the molecule from dissociation and the recombinant emission over the various electronic states that correlate with O (^3P) + O (^3P) is observed [10,11]. Due to the light mass and week forces in the quantum solid of hydrogen, we would expect significantly reduced stopping power of the host. Whether O_2 will undergo facile photodissociation under 193 nm irradiation in solid hydrogen is

the first question of interest. Quite clearly, in addition to the different kinematics of quantum versus classical solids, now reactive channels for formation of OH and H_2O are open to the photodissociation of O_2. The laser induced fluorescence (LIF) probes used in our experiments give no evidence to the presence of these reactive channels, we only detect molecular and atomic oxygen, and in both cases only a fraction of the population is detected. We have previously reported on the spectroscopy of molecular O_2 isolated in solid hydrogen and deuterium [12]. We rely on the orbitally forbidden $A'(^3\Delta_u)$–$X(^3\Sigma_g^-)$ transition, known as the Herzberg III band [13], as the laser induced fluorescence probe of the isolated molecules. This transition gains its intensity by matrix induced mixing between O_2 (A') and the nearby repulsive O_2 $(^3\Pi)$ state. Based on the symmetry requirements for the mixing, we have argued that only molecules isolated in fcc sites and oriented along the [111] axis of the unit cell are observable. Only a fraction of the molecules are observable in solid D_2, and none are detectable in solid H_2, although the presence of the isolated molecules could be verified there by thermal cycling of solids over-coated with a film of Xe. It was inferred that in solid H_2 the guest O_2 molecules are exclusively isolated in hcp sites. This consideration is the main reason for carrying out the present studies in solid D_2, in which metastable fcc sites can be produced via thermal cycling. In rare gas solids both atomic and molecular oxygen can be monitored through fluorescence induced by laser irradiation at 193 nm. The same applies in solid D_2; although, as will be argued, this non-resonant probe is also limited to detection of special sites. Nevertheless, the availability of a method to monitor O atoms, via its O $(^1S \rightarrow {}^1D)$ emission, allows verification of its photogeneration, and allows direct conclusions with regard to chemical stability and thermal induced recombination. As will be discussed, we find the concept of an atomic impurity diffusing through the solid lattice to be misguided. The more surprising result is the absence of chemistry on the $O(^1D) + H_2$ potential energy surface, which in gas phase binary collisions would lead to formation of OH + H [14], but in the presence of third body should form H_2O. According to the most refined potential energy surfaces the gas phase reaction is barrier free [15]. To ensure that the solid state observations of non-reactivity were not a peculiarity of the special sites probed, we carry out measurements in solid D_2 co-doped with O_2 and Xe, in which Xe acts as a sensitive detector of atomic oxygen in its various electronic states [16]. These studies more definitively confirm the chemical stability of O (^1D) in solid D_2. This unexpected result could not be rationalized in molecular dynamics calculations using refined, non-additive, but covalent pair potentials [6]. However, the more recent theoretical treatment, using the diatomics-in-molecules approach which takes into account the ionicity of interactions, succeeds in providing a rationale for the many-body origin of the reaction barrier [17]. Here we provide the experimental data that has inspired these theoretical developments.

2. Experimental

We prepare the doped films by spray-deposition of premixed gaseous samples on an oxygen free copper substrate, mounted on the cryotip of a He flow-cryostat (see schematic in Fig. 1). The cryostat is contained in an all stainless steel, ultra-high vacuum shroud fitted with metal sealed MgF_2 and sapphire windows. A silicon diode of ± 0.05 K accuracy (Lakeshore Cryotronics) mounted on the back-side of the copper substrate, is used for temperature measurements. The shroud is evacuated with a turbo-molecular pump to a base pressure below 10^{-8} Torr at room temperature. The samples are deposited at temperatures ranging from 3.8 K to 5.5 K, with film growth rates ranging from 1.6 μm/min to 3.6 μm/min. The sample thickness

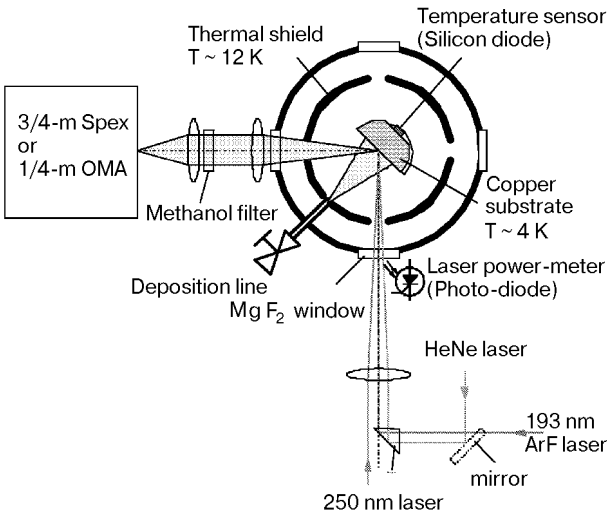

Fig. 1. Experimental setup. The He flow cryostat is adapted for simultaneous monitoring of fluorescence induced by the 193 nm laser and the doubled dye laser from the same interrogation volume. The temperature of the cryotip is monitored with a Si-diode, the output of which is read-out by the computer, along with the fluorescence and thermoluminescence data. The He : Ne laser is used to monitor thickness of the growing film, otherwise the films are invisible to the eye.

is measured during deposition by monitoring interference fringes from a reflected He : Ne laser. Typical film thicknesses vary from 50 to 100 μm. The films are transparent to the eye.

Emission from the sample is recorded using either an optical multichannel analyzer (Princeton Applied Research OMA3) equipped with a 0.25-m polychromator, or using a photomultiplier (Hamamatsu R-666) after dispersing the radiation through a 0.75-m monochromator (Spex). A digitizing/averaging scope (Tektronics 2430) is used to record transients, which are then transferred to a personal computer for further data analysis. The same computer is also interfaced to the temperature sensor/controller and the time delay generator used to synchronize the lasers.

As excitation source, the doubled output of an excimer pumped dye laser and/or the direct output of an ArF laser operating at 193 nm is used. In many of the experiments the two lasers are synchronized to correlate resonantly induced fluorescence from the molecules with 193 nm induced chemistry and fluorescence of atomic and molecular oxygen.

3. Results

O_2 *doped solid* D_2

The majority of experiments were performed in oxygen doped solid deuterium samples with a gas mix composition of 1 : 500. Excitation of O_2/D_2 samples at 193 nm leads to emission on both molecular O_2 ($A'^3\Delta_u \rightarrow X^3\Sigma_g$) and atomic O ($^1S \rightarrow {}^1D$) transitions, as shown in Fig. 2,*a*. The fluorescence lifetime of the molecular emission is 5.4 μs, while that of the atomic emission at 559 nm is 230 μs (measured at 4 K). In addition to this LIF scheme, the photo-generation of O atoms can be verified through their thermoluminescence (TL). The thermally driven recombination of atoms, O (^3P) + O (^3P), produces the same $A' \rightarrow X$ spectrum, as shown in Fig.2,*b*. The same emission spectrum is obtained through resonant $A' \leftarrow X$ excitation of the molecule, as previously described in some detail [12]. Note, the fluorescence yield of the resonant excitation depends on structural changes of the solid, since it probes only a sub-ensemble of molecules in fcc sites. Also, the 193 nm induced molecular emission is contingent upon cage induced recombination of the atoms, and therefore not a direct probe of the molecular concentration. Further, the excitation resonance responsible for the 193 nm induced atomic emission is not clear. We can establish that the atomic emission arises from a broad structureless absorption. This is illustrated in Fig. 3 and contrasted with the sharp molecular resonances in the same spectral range. A search for direct access of the emitting atomic state, via the forbidden $^1S \leftarrow {}^3P$ transition near 297 nm, failed. Thus, the 193 nm probe of the O atoms is also indirect, and as will further be shown, not a quantitative probe of the atom concentration in the solid.

To correlate the thermal and irradiation histories of the atomic and molecular fluorescence, we simultaneously monitor LIF from the 193 nm laser and the doubled dye laser. The latter is tuned to the molecular A' ($v' = 8$) $\leftarrow X$ ($v'' = 0$) resonance at 249.33 nm, the lasers are delayed by 1 ms relative to each other, and the fluorescence is gate-detected to distinguish the various contributions. Figures 4 and 5 illustrate typical histories in «quench» condensed samples, prepared by slow deposition at the lowest temperature of the cryostat of 3.8 K. The data illustrate that:

a) In the freshly deposited samples, at 3.9 K, 193 nm irradiation does not cause a measurable change in either the resonantly induced O_2 emission

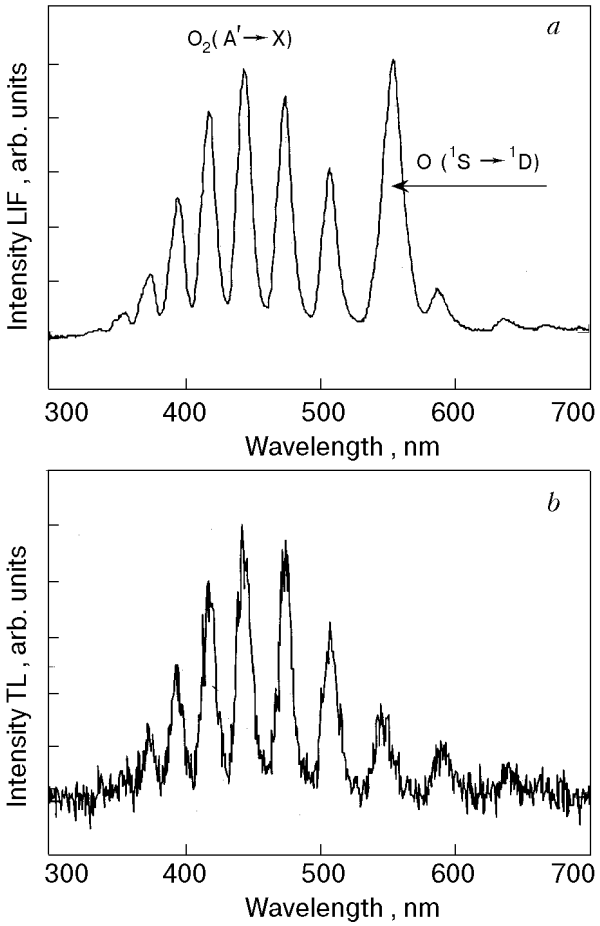

Fig. 2. Laser induced fluorescence (*a*) and thermoluminescence (*b*) from O_2 doped D_2 solids irradiated at 193 nm. The atomic O ($^1S \rightarrow {}^1D$) emission, at 559 nm, appears in the laser induced fluorescence spectrum in (*a*).

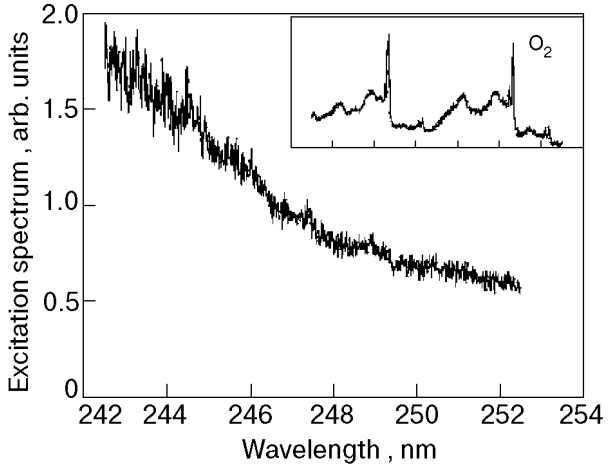

Fig. 3. Excitation profile of the atomic O ($^1S \rightarrow {}^1D$) emission. In the inset, the excitation spectrum for the molecular O_2 ($A' \rightarrow X$) emission is shown.

(Fig. 4), or in the 193 nm induced atomic and molecular emissions (Fig. 5).

b) Upon warming the sample to 5.5 K with continued irradiation, a sudden, tenfold growth in the 193 nm induced molecular and atomic emissions are observed. This is accompanied by a sudden, 90%, loss of the resonantly induced molecular emission. This sudden transition suggests gross structural change in the lattice. With continued irradiation, the 193 nm induced emission decays in time, while the resonantly induced emission does not recover. Clearly, the O_2 molecules probed by the two different lasers, belong to two different ensembles. The 193 nm induced decay is verified to be laser aided, by noting that when the irradiation is interrupted the emission intensity remains constant. The level to which the emission decays is temperature dependent. When the temperature is lowered to 4 K, the emissions subside to pre-warm-up level.

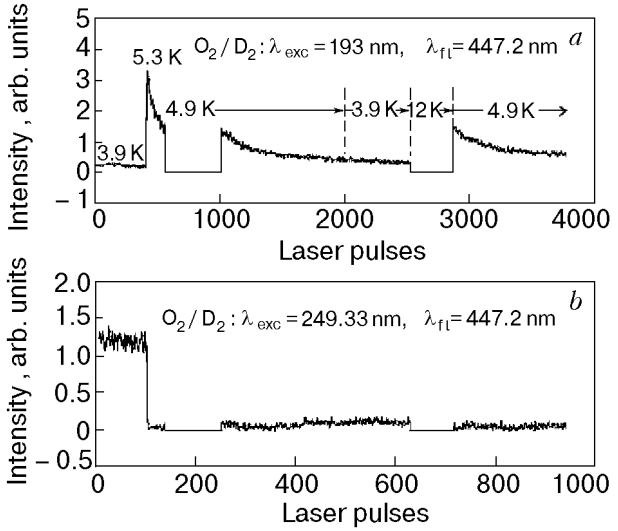

Fig. 4. Thermal and irradiation histories of molecular laser induced fluorescence in a quench-condensed solid. The sample, 0.2% O_2 in solid D_2 , was deposited at 3.8 K. The temperature is varied during irradiation, and it's history is indicated in (*a*). The flat regions centered at 200 and 700 pulses of the 249 nm laser, correspond to periods where the laser beams were blocked off.

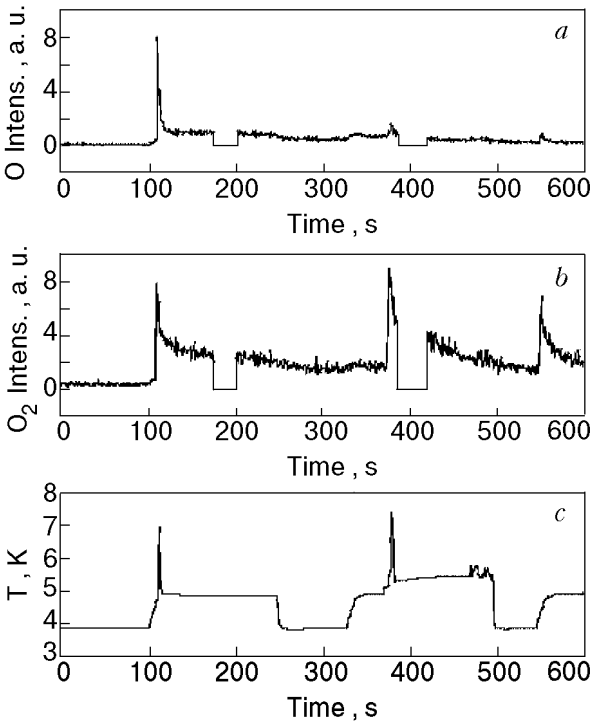

Fig. 5. Thermal and irradiation histories of 193 nm induced atomic (*a*) and molecular (*b*) fluorescence in the quench-condensed solid (0.2% O_2 in solid D_2). The thermal runaway spike is associated with gross change in the morphology due to phase transition of islands in the solid (*c*).

c) The resonantly induced molecular emission does not respond when the warm-up cycle is repeated (Fig. 4). The 193 nm induced molecular emission repeats its behavior (Fig. 5,*b*), and the atomic emission does not fully regenerate in subsequent cycles (Fig. 5,*a*).

d) Note the thermal runaway at 5.3 K, as evidenced by the temperature spikes in Fig. 5,*c*. They repeat at the same temperature, and are clearly independent of the atom content of the solid. This behavior is consistent with the known reversible, hysteretic phase transition of quench-condensed solid deuterium [18]. The initial 90% drop in the resonantly induced molecular fluorescence can therefore be understood as due to fcc to hcp phase transition in crystallites. The transition evidently generates sites in which the 193 nm induced O_2 fluorescence is observed.

A substantively different behavior is observed in samples deposited at higher temperature, between

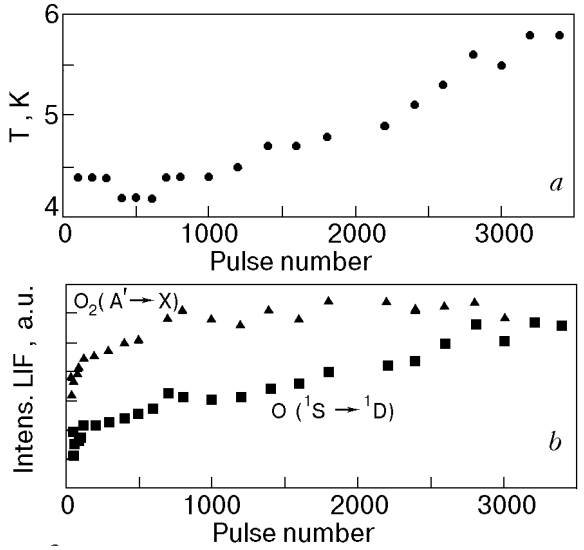

Fig. 6. Thermal (*a*) and irradiation (*b*) history of an $O_2 : D_2$ sample deposited at 5 K and annealed at 9 K, prior to irradiation. The data points are the 193 nm induced fluorescence from O and O_2 as a function of number of pulses of the laser.

4.5 K and 5.5 K. An example is shown in Fig. 6 for a sample deposited at 5 K, annealed at 9 K, then slowly cooled to 4.4 K to start the radiation process. A correlated growth of both atomic and molecular fluorescence is observed upon 193 nm irradiation at 4.4 K. As the temperature is increased to 6 K with continued irradiation, both atomic and molecular emissions grow. As long as the temperature is held constant, these emissions remain stable at this level.

In principle, glow curves obtained by a programmed temperature ramp should enable the characterization of diffusion and recombination kinetics of atoms. This method has previously been implemented successfully for atomic oxygen in rare gas solids [8]. We have failed to obtain any meaningful glow curves in solid D_2 . The recombination occurs suddenly, leading to a flash that lasts only ~ 10 μs. The flash is always accompanied with temperature and pressure surge, similar to the laser induced fluorescence spikes shown in Fig. 5. The temperature at which the catastrophic recombination occurs depends on the gross sample morphology, determined mainly by sample deposition conditions. In samples prepared by slow deposition at 3.8 K, the recombination occurs between 5.5 K and 7.5 K. In samples deposited at somewhat higher temperatures, 4.5 K–5.5 K, and at a deposition rate of ~ 3 μm/min, the recombination occurs at a temperature between 7 K and 9 K. In samples which are pre-annealed at 9 K, then cooled to 4 K and irradiated, the TL is observed at temperatures as high as 11 K.

N_2O *doped solid* N_2 *and neat solid* O_2

Extensive 193 nm irradiation of N_2O doped solid N_2 (M/R = 1:1000) and neat solid O_2 did not produce any detectable emission from atomic O. Given the fact that N_2O dissociates readily in solid N_2 [19], the absence of 193 nm induced O atom emission supports the notion that the atomic LIF observed in solid D_2 arises from special centers. The absence of 193 nm induced atomic emission in solid O_2 establishes that the observed emission in solid D_2 is not from clusters of O_2 .

Solid D_2 *co-doped with* O_2 *and* Xe

To avoid the uncertainty of LIF detected O atoms in solid D_2 , we carried out a set of studies in ternary solids prepared at a mole ratio of 1:5:500 O_2:Xe:D_2 . After depositing the samples at 5 K, the O_2 excitation spectra were investigated with the doubled dye laser. The excitation and emission spectra of O_2 are identical to that obtained in the absence of Xe, indicating that only isolated molecules are interrogated in both cases. This is consistent with the fact that the $A' \to X$ emission is quenched by Xe. Excitation at 193 nm immediately

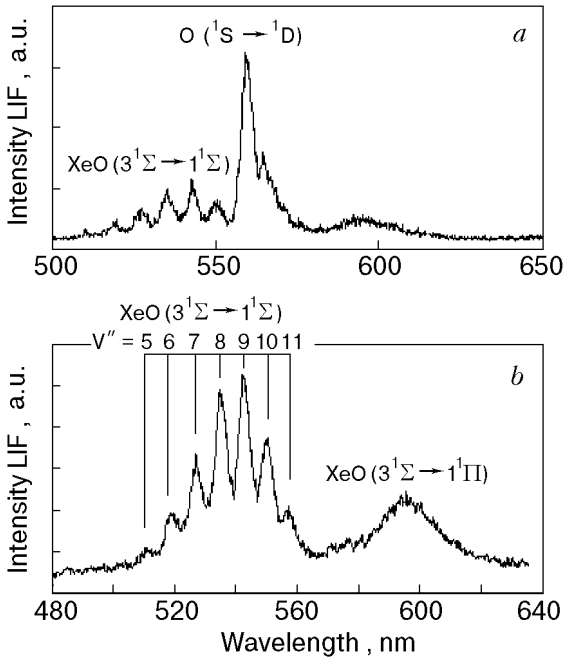

Fig. 7. Fluorescence spectrum obtained with 193 nm irradiation of solid D_2 co-doped with O_2 and Xe (O_2 : Xe : D_2 = 1:5:500). The spectrum (*a*) is obtained with time integration, the spectrum (*b*) is obtained with a 100 ns gate. All features in the spectrum (*b*) have the same lifetime of (130±5) ns, while the atomic oxygen emission (*a*) has a lifetime of 50 μs.

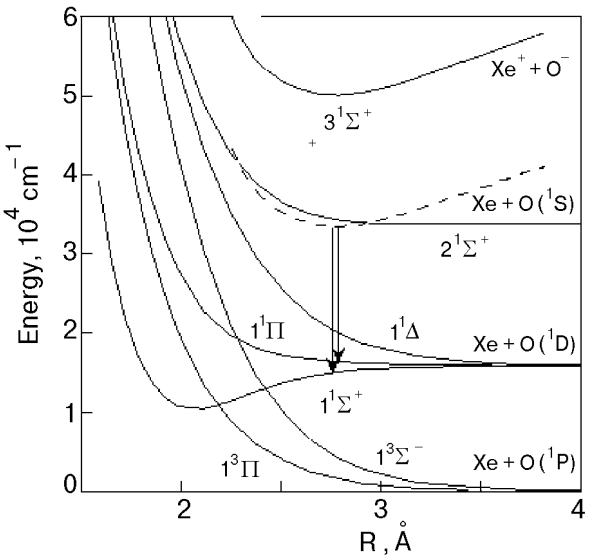

Fig. 8. The gas phase XeO potentials and the required placement of the upper emitting state (dashed line) in the fluorescence spectrum of Fig. 7. Note, a double minimum is implied to arise from the mixing between $3\,^1\Sigma$ and $2\,^1\Sigma$ potentials.

produced a bright emission from XeO centers, as illustrated in Fig. 7. The molecular fluorescence induced at 193 nm, which was the dominant feature in the O_2/D_2 samples (see Fig. 2) is practically absent in the spectrum of Fig. 7. The spectrum now consists entirely of atomic emissions. In the time integrated spectrum, the O ($^1S \rightarrow {}^1D$) emission can clearly be identified. While the peak is virtually unshifted at 559 nm, the effect of Xe is to reduce the radiative lifetime to 50 μs (230 μs in D_2). Thus, it may be more appropriate to assign this transition to XeO ($2\,^1\Sigma \rightarrow 1\,^1\Sigma$) [20]. In addition, a vibrational progression centered at 530 nm and a broad band at 590 nm, are observed. Both of these emissions have lifetimes of (130 ± 5) ns. Accordingly, they can be separated from the atomic emission by gated detection, as shown in the Fig. 7,*b*. With the help of the Xe–O potential energy curves illustrated in Fig. 8, the nature of these emissions can be identified with some confidence [21]. Given that the vibrational progression and the band at 590 nm have the same lifetime, they are likely to originate from the same upper state. Given their short radiative lifetime, they can be confidently assigned to the $Xe^+O^- \rightarrow XeO$ charge transfer transitions. Given that only the XeO ($1\,^1\Sigma$) state, which correlates with O (^1D) + Xe ($^1S_0$), is deep enough to sustain the vibrational progression, the transition can safely be assigned to Xe^+O^- ($3\,^1\Sigma$) → XeO ($1\,^1\Sigma$). This would then suggest that the broad emission at 590 nm is due to Xe^+O^- ($3\,^1\Sigma$) → XeO ($^1\Pi$). In both cases the terminal state of the transition correlates with O (^1D) + Xe ($^1S_0$). The vibrational progression seen here is quite similar to that observed for XeO in solid Ar [22], and the numbering is simply taken from there.

While monitoring the 193 nm induced fluorescence of the atomic centers, the samples were warmed up. The emission stays nearly constant up to 12 K, and permanently decays as D_2 starts to evaporate. These samples do not show significant TL, presumably because $O_2(A')$ is quenched by Xe. All recombination must occur at Xe sites as the D_2 evaporates.

4. Discussion

The non-reactivity of O (^1D)

The interpretation of the experiments in $O_2/Xe/D_2$ is the most direct with regard to the chemical stability of atomic oxygen in its various electronic states in solid D_2 . The observation of the molecular resonant excitation immediately after deposition, establishes the presence of isolated molecules. Subsequent irradiation at 193 nm, generates the O and XeO emissions, without a trace of the molecular spectrum. We may conclude that O_2 can be photodissociated in solid D_2 by 193 nm irradiation. Despite the excess energy of 1.3 eV, the impulsively generated O (^3P) atoms survive in the D_2 host. The absence of any 193 nm induced recombinant molecular fluorescence is a good indication that the cage is ineffective in solid D_2 .

The O atoms scavenged by Xe are interrogated via the XeO charge transfer transitions, which can be assigned with some confidence. They invariably terminate on the O (^1D) + Xe potential energy surface. We can be sure that the O : Xe pair is surrounded by D_2 , since in Xe clusters the XeO emissions occur at 740 and 370 nm [7]. The fact that the XeO transitions do not bleach with extended irradiation, establishes that the photogenerated O (^1D) atoms do not react with the host.

It would seem that the vicinity of Xe atoms is sufficient to generate a barrier toward the O (^1D) + + D_2 reaction. This barrier cannot be due to the binding between O (^1D) and Xe, since at least in the 559 nm transition, which is red shifted from the gas phase value of 557.7 nm, the transition must terminate on the flat part of the interaction potential. The perturbation that may be ascribed to Xe is the change in transition dipole of the atomic $^1S \rightarrow {}^1D$ emission, evidenced by the shortening of the radiative lifetime to 50 μs. The origin of this perturbation is well understood to be due to the ionicity of the XeO ($2\,^1\Sigma$), which is derived by

mixing with the Xe^+O^- ($3\,^1\Sigma$) charge transfer state. Indeed, to rationalize the observed emission spectra of the charge transfer states, we must conclude that due to solvation in the polarizable medium, the Xe^+O^- ($3\,^1\Sigma$) and XeO ($2\,^1\Sigma$) potentials are strongly mixed. The situation is quite similar to that of XeO in solid Ar (which has polarizability similar to that of H_2) for which we had suggested the creation of a double minimum due to the crossing of the solvated Xe^+O^- ($3\,^1\Sigma$) and XeO ($2\,^1\Sigma$) potentials [7]. This is shown schematically in Fig. 8. Note, the double-minimum can arise by mixing between the charge transfer and covalent state, rather than the creation of an actual crossing which would require the lowering of the Xe^+O^- ($3\,^1\Sigma$) state by ~ 1.5 eV [21]. The fact that the radiative lifetime of the transition is 130 ns, is sufficient to identify the nature of the transition as that of charge transfer, and therefore the upper state as Xe^+O^-. Why would this prevent chemistry on the terminal O (^1D) + D_2 surface? We surmise that the partial charge in $Xe^{\delta+}O^{\delta-}$, prevents the formation of the O–H bond, which can only proceed by developing positive charge on the targeted hydrogen molecule. In effect, the partial charge transfer on the Xe + O (^1D) can be thought to create a polarization barrier. This is the essence of the theoretical analysis of O doped solid H_2 which we consider next [17].

Consider the O ($^1S \rightarrow {}^1D$) transition in D_2, in the absence of Xe. Independent of the excitation channel, since this emission does not bleach, we have to conclude that atomic oxygen in all of its electronic states, and in particular in its ^1D state, does not react with the host. This, at first, seems at odds with the well established fact that the O (^1D) + H_2 surface does not contain a reaction barrier. The diatomics in molecules (DIM) calculations of Kunz, in which $O(H_2)_n$ is considered with the explicit inclusion of the ionic manifold of states for the cluster, show the many-body nature of the barrier [17]. The picture is as follows: The O (^1D)–H_2 interaction gains its binding character due to its ionicity. When in the middle of an octahedral array of H_2 molecules, the central O atom can mix with the charge transfer states of all neighbors. The insertion coordinate, however, requires the localization of charge on one hydrogen molecule to reach the ionicity of the O–H bond in its H–O–H transition state. The barrier arises as the energy of localization of the excited state charge density, from the 12 nearest neighbors to one molecule. The charge distribution in the excited state is mirrored by the polarization on the ^1D-surface. In effect, the polarization barrier centers the O atom in the cubic site, and prevents the reaction. In the absence of the many, there is no barrier. To our knowledge, this is the most direct demonstration of a many-body-potential control of chemical dynamics.

Non-resonant excitation mechanism: O_2 (X) : O (^3P) *centers*

Although 193 nm excitation is used to follow both O and O_2 in solid D_2, the mechanism of this excitation is indirect, preventing quantitative determinations of impurity concentrations and photodissociation yields. The excitation spectrum in Fig. 3 indicates that the atoms are accessed through a broad band, that cannot be ascribed to the isolated atom, but rather to an M–O adduct, similar to the charge transfer states of Xe–O. Similarly, the observation that the 193 nm induced molecular emission grows with irradiation time, as seen in Fig. 6, clearly indicates that we are not simply interrogating the molecular concentration. The close correlation of the thermal and irradiation histories of 193 nm induced O and O_2 emissions suggests a common origin. The most consistent assignment that can be offered is that the absorption is due O_2 (X) : O (^3P) pairs, distinct from ozone. Since both O and O_2 are present in the sample, O_3 can be formed. However, the excitation wavelengths used, 193 nm–255 nm, do not have the requisite energy to produce O (^1S) from the ground state of ozone, and cannot therefore explain the LIF signal over the O ($^1S \rightarrow {}^1D$) transition. The main dissociation channel of ozone in this excitation range is the production of O (^1D) [19]. As in the case of N_2O and O_3 isolated in rare gas solids, we expect that ozone would undergo facile photodissociation in solid D_2. Even though the magnitude is difficult to obtain with confidence, *ab-initio* calculations invariably show an angle dependent potential barrier to formation of O_3 from O_2 (X) : O (^3P) [23,24]. A continuous excitation spectrum, starting near 250 nm, can then be ascribed to absorption over the dense manifold of inter-molecular O_2–O potentials, from which branching to O_2 + O (^1S) and to O_2 (A') + O is to be expected.

The above consideration complicates the interpretation of 193 nm driven photodissociation yields of O_2 in solid D_2. The samples containing Xe indicate facile dissociation, accompanied with migration of O atoms to reach the Xe sites. In the absence of Xe, we cannot establish photodissociation probabilities, or equivalently, the caging efficiency of the host, since the observed atomic and molecular densities can entirely be attributed to special centers. Indeed, in samples where LIF from

the atomic centers is nearly absent, a strong thermoluminescence is observed upon warm-up, indicating that only a fraction of the O atoms are spectroscopically detected. Nevertheless, it is clear that chemistry, namely formation of H_2O, is not a significant channel in the dissociative excitation of O_2 .

Thermal induced recombination

The thermal induced recombination of oxygen atoms in solid D_2 fundamentally differ from what is observed in the classical rare gas solids. There, it is always possible to ramp-up the temperature at a rate at which the glow curve can be measured, to extract the diffusion kinetics of impurities in the solid. This is not possible in the solid hydrogens. Instead of a glow curve, we obtain a sudden flash, accompanied by uncontrollable thermal runaway and pressure surge. In effect, the host diffuses around the impurities. The theoretical analysis of O doped solid hydrogens gives a useful perspective [6]. Due to the deeper guest-host potential, hydrogen molecules are significantly more localized near the impurity site. In fact, a linear increase in the density of the solid is predicted as a function of concentration of O atoms. In effect, the O atoms are coated with a layer of hydrogen, which is less mobile than the bulk. It would therefore be difficult to imagine the coated impurity diffusing while the host retains its integrity as a solid. The experimental observation is rationalized as the fusion of O centers in a solid undergoing gross structural change due to self-diffusion of the host, with the recombination energy of the guests serving as positive feedback for the thermal runaway.

5. Conclusions

Atomic oxygen can be photogenerated in-situ in solid D_2 by photodissociation of molecular oxygen. The atomic centers in such a solid are stable, both chemically and physically. The non-reactivity of O (^1D) with the host is particularly striking, and rationalized to result from a polarization barrier of strictly many-body origin [17]. In pre-annealed samples, the atomically doped solids have been shown to be stable up to $T = 11$ K. Indeed, in earlier simulations it had been argued that atomic oxygen stabilizes the host lattice, and increases its density [6]. This is indirectly verified in the present, by recognizing that O atoms recombine only after the host loses its integrity as a solid. Thus, this exploratory study seems to resolve some of the more rudimentary issues with regard to the consideration of oxygen doped solid hydrogen as a propellant. In this regard, the experiments do not provide a reliable estimate of the concentration of atomic centers, or the achievable doping levels, considerations crucial to assess specific impulse.

The spectroscopy, photodynamics, and photophysics of impurities in solid hydrogens raise many fascinating questions. A more quantitative study of the very system we have described, for example by combining IR and visible methods, would be quite useful. The present studies remain qualitative with regard to several important questions. With regard to the caging ability of the solid, based on the O_2 : Xe : D_2 experiments, we believe it to be small. Based on the thermal and irradiation histories of fluorescence we have postulated the presence of O_2 (X) : O (^3P) pairs that do not form ozone. Infrared studies could nicely resolve this issue. More generally, solid hydrogen could be used as an ideal non-perturbing medium of weak forces to investigate intermolecular potential energy surfaces [25]. Finally, in the present study the effects of ortho- and para-hydrogen have been completely neglected. They need not be invoked to explain any of the observations, and it is believed that due to the paramagnetic nature of the impurities, at the concentrations of impurities used, the solid host is entirely in the ground spin state.

Acknowledgements

This research was supported through grants from the US AFOSR, S04611-90-K-0035 and F49620-95-1-0213. We thank the Ministry of Education of Japan for support to H.K. and S.T. during their stays in Irvine. The discussions with P. Kuntz, which resulted in his DIM treatment of O (^1D) in H_2 , have been quite fruitful. We thank M. Petterson for his critical comments and discussions, and N.T.A. for help with graphics.

1. P. G. Carrick, *Specific Impulse Calculations of High Energy Density Solid Cryogenic Propellants 1: Atoms in Solid* H_2 , report PL-TR-93-3014, of the Propulsion Directorate of the Phillips Laboratory, USAF, (1993).
2. The same general motivation had earlier resulted in the Broida report: *Formation and Trapping of Free Radicals*, A. M. Bass and H. P. Broida (eds.), Academic Press (1960).
3. V. A. Apkarian, *Proceedings of the High Energy Density Matter (HEDM)* Conferences of the USAF, Woods Hole (1995); *ibid.* Z. Li and V. A. Apkarian, Boulder (1996); *ibid.* V. A. Apkarian, Washington DC (1997).
4. A. V. Danilychev, *Ph. D. Thesis*, UC Irvine (1994).
5. M. Sterling, Z. Li, and V. A. Apkarian, *J. Chem. Phys.* **103**, 5679 (1995); Z. Li and V. A. Apkarian, *J. Chem. Phys.* **107**, 1544 (1997).
6. Z. Li, V. A. Apkarian, and L. B. Harding, *J. Chem. Phys.* **106**, 942 (1997).

7. W. G. Lawrence and V. A. Apkarian, *J. Chem. Phys.* **97**, 2229 (1992).
8. A. V. Danilychev and V. A. Apkarian, *J. Chem. Phys.* **99**, 8617 (1993).
9. A. V. Danilychev and V. A. Apkarian, *J. Chem. Phys.* **100**, 5556 (1994).
10. A. C. Becker, U. Schurath, H. Dubost, and J. P. Galaup, *Chem. Phys.* **125**, 321 (1988).
11. S. Koda and H. Kajihara, *Bull. Chem. Soc. Jpn.* **70**, 1225 (1997); H. Kajihara, T. Okamura, and S. Koda, *Chem. Phys. Lett.* **256**, 126 (1996); H. Kajihara, T. Okamura, F. Okada, and S. Koda, *Laser Chemistry* **15**, 83 (1995).
12. A. V. Danilychev, V. E. Bondybey, V. A. Apkarian, S. Tanaka, H. Kajihara, and S. Koda, *J. Chem. Phys.* **103**, 4292 (1995).
13. G. Herzberg, *Can. J. Phys.* **31**, 657 (1953).
14. For a most recent study, see: M. Alagia, N. Balucani, L. Cartechini, P. Casavecchia, E. H. vanKleef, G. G. Volpi, P. J. Kuntz, and J. J. Sloan, *J. Chem. Phys.* **108**, 6698 (1998).
15. G. C. Schatz, A. Papaioannou, L. A. Pederson, L. B. Harding, T. Hollebeek, T. S. Ho, and H. Rabitz, *J. Chem. Phys.* **107**, 2340 (1997).
16. L. R. Leclair and J. W. Mcconkey, *J. Chem. Phys.* **99**, 4566 (1993).
17. P. J. Kuntz, *Chem. Phys.* **240**, 19 (1999).
18. H. Meyer, *Physica* **B197**, 360 (1994).
19. A. V. Benderskii and C. A. Wight, *Chem. Phys.* **189**, 307 (1994).
20. T. H. Dunning and P. J. Hay, *J. Chem. Phys.* **66**, 3767 (1977).
21. For a recent study of the XeO potentials, see: M. Yamanishi, K. Hirao, and K. Yamashita, *J. Chem. Phys.* **108**, 1514 (1998).
22. J. Goodman, J. C. Tully, V. E. Bondybey, and L. E. Brus, *J. Chem. Phys.* **66**, 4802 (1977).
23. A. Banichevich, S. D. Peyerimhoff, and F. Grein, *Chem. Phys. Lett.* **173**, 1 (1990).
24. G. J. Atchity and K. Rudenberg, *Theor. Chem. Acc.* **96**, 176 (1997).
25. Simon Tam and Mario E. Fajardo, *Fiz. Nizk. Temp.* **26**, 889 (2000).